


Restoration of the inferomedial orbital strut using a standardized three-dimensional printing implant

Jun Hyeok Kim,^{1,*}  In-Gyu Lee,^{2,*} Jeong-Seok Lee,² Deuk Young Oh,¹ Young Joon Jun,¹ Jong Won Rhie,¹ Jin-Hyung Shim^{2,†} and Suk-Ho Moon^{1,†} 

¹Department of Plastic and Reconstructive Surgery, College of Medicine, Catholic University of Korea, Seoul, Korea

²Department of Mechanical Engineering, Korea Polytechnic University, Siheung, Korea

Abstract

The inferomedial orbital strut (IOS) is the thin bony junction of the orbital medial wall and floor. Its fracture is common and leads to serious complications, including enophthalmos, globe dystopia and diplopia. However, anatomical restoration of the IOS is challenging owing to reduced structural support; sound anatomical background and accurate implants are therefore essential. The aim of the present study was to incorporate data from cadaveric orbit anatomy into three-dimensional (3D) printing technology and to reconstruct the complex orbital fracture elaborately. After averaging the data from computed tomography (CT) images of 100 adult cadavers, the dimensions of the IOS were extracted, and a tangent sphere was created using a computer-aided design program. The curves were compared with the CT data of 10 adult patients from the simulation test. Based on these data, a standardized 3D implant, 1.15 mm thick, was designed using polycaprolactone. The implant was placed in five patients with complex orbital fractures. The radius of the sphere in contact with the orbit, measuring 33.54 mm, was confirmed to be appropriate. A comparison between the normal side volume (V_0) and the postoperative volume (V_{post}) showed that they were statistically similar. Furthermore, a comparison between V_0 and the preoperative volume (V_{pre}), and V_{post} compared with V_{pre} also showed a statistically significant difference ($P < 0.05$). On follow-up, the preoperative ocular symptoms were resolved. The orbital data obtained from 100 cadavers provided standardized orbital anatomy, and 3D printed implants were created. The implants were anatomically accurate with regard to the orbital cavity and adequately covered the simulation model. The implant also showed satisfactory results when applied clinically in actual patients.

Key words: inferomedial orbital strut; orbital fracture; 3D printed implants; computer-aided design.

Introduction

The inferomedial orbital strut (IOS) is the thin, triangular bony junction of the orbital medial wall and floor (Yao et al. 2016). The orbital medial wall and floor are the two

most frequently fractured sites of the orbit (Hur et al. 2015), and complex fractures involving the IOS are common (Manolidis et al. 2002; Gooris et al. 2017). The IOS represents a crucial anatomical area in the orbit, and its fracture can result in serious and visible enophthalmos, globe dystopia and diplopia (Goldberg et al. 1992; Wright et al. 1999; Jordan & Anderson, 2000; Stathopoulos & Ameerally, 2018).

Reconstruction of the supportive bony structures from the orbital medial wall through the IOS to the floor is crucial (Burnstine, 2003; Jaquier et al. 2007; Gart & Gosain, 2014; Bartoli et al. 2015); however, anatomically precise restoration of the IOS is challenging because the IOS is a conceptual structure consisting of the maxillary bone, aerated ethmoid bone and palatine bone; its thickness and hardness vary depending on the location (Kim et al. 2002). As the fracture of the IOS leads to lack of structural support, appropriate placement of the implant is compromised (Su & Harris, 2006; Hur et al., 2015). Precise anatomical knowledge of the IOS is therefore essential for restoration of the orbit.

Correspondence

Suk-Ho Moon, Department of Plastic and Reconstructive Surgery, Seoul St Mary's Hospital, College of Medicine, Catholic University of Korea, 222 Banpo-daero, Seocho-gu, Seoul 06591, Korea.

E: nasuko@catholic.ac.kr

Jin-Hyung Shim, Department of Mechanical Engineering, Korea Polytechnic University, 237 Sangidaehak-Ro, Siheung-Si, Gyeonggi-Do 15073, Korea. E: happyshim@kpu.ac.kr

*J.H. Kim and I.G. Lee contributed equally to this work as the first author.

†J.H. Shim and S.H. Moon contributed equally to this work.

Accepted for publication 19 November 2019

Article published online 18 December 2019

In the present study, anatomical restoration of the fractured IOS was attempted by creating a suitable implant using three-dimensional (3D) printing technology. The orbital implant created reproduced the curvature of the IOS using anatomical data, which were established by standardizing radiological images of 100 cadavers.

Materials and methods

Analysis of the orbital inferomedial curvature based on Korean standard data

Standard data were established based on the data obtained from the computed tomography (CT) images of 100 samples from Korean adult donors (50 men and 50 women) provided by the Korea Institute of Science and Technology Information (KISTI; Seung-Ho et al. 2006; <http://dk.kisti.re.kr>).

The donated cadavers, which had no bone damage, were donated to nine university hospitals. The mean (range) ages at death were 50.3 (21–60) years for the men and 54.3 (27–60) years for the women, and the mean (range) heights were 166 (159–178) cm for the men and 156 (146–166) cm for the women. These were within the range of Korean standards.

Four-channel CT was performed at intervals of 1 mm to obtain cross-sectional images, and a 3D human model was established for male and female bones by KISTI. Each of the individual bone shape models adopted an averaging technique sequence to identify the centre of mass, alignment of direction, scaling, and averaging to produce an averaging model for the skeletons of men and women. An averaged individual bone shape model was reconstructed to suit the anatomical locations in order to build a sample skeleton model of the average male and female Korean.

Thereafter, 3-matic (Materialize, Belgium), a 3D computer-aided design program, was used to extract the dimensions of the IOS from the orbital medial wall to the floor of the skull, including the orbital surface of the maxilla, lacrimal bone, ethmoid bone, sphenoid bone, palatine bone and zygomatic bone. Using the standard data, a sphere in contact with the IOS was created, and the radius was measured (Fig. 1). After calculating the mean curvature from the measured radius, a standardized sphere was generated.

The present study was approved by our institutional review board (Catholic Medical Centre Office of Human Research Protection Program; KC18RESI0384).

Simulation of the standardized implant

To verify the reliability of the averaged curves reflecting the shape of the IOS, the generated sphere was simulated by applying it onto the patient model based on the CT data of normal adults (five men, five women) who had no trauma or disease above the neck. Using the 3D image-processing software Mimics (Materialize), the skull, including its orbit, was visualized in three dimensions, and the standardized sphere was simulated by being placed on the IOS of the orbit. Through standardized modeling, the implant design was expanded from the curvature to the medial wall and floor. The distance between each point of the implant and the simulation model was measured to determine the accuracy of the fit and to verify the appropriateness of the implant design on the orbital wall.

Production of the Korean standardized orbital mesh implant using 3D printing technology

The standardized implant was 1.15 mm thick and was created with 3D printing technology (TnR Mesh [Orbital type]; T&R Biofab Co., Ltd, Seoul, Korea) using the biocompatible polymer, polycaprolactone (PCL), which is non-toxic, absorbable and absorbent (Cho, 2014; Teo et al. 2015). PCL implants are radiolucent and semi-rigid materials with structural stability.

Clinical application

The fabricated implant was applied in patients with orbital complex fractures, as confirmed on the CT or during surgery. Surgery was performed via subciliary and transcaruncular approaches under general anesthesia.

After the subciliary skin was incised, the septum was dissected from the orbicularis oculi muscle toward the infraorbital rim. Then, a transcaruncular incision was created between the orbital septum and Horner's muscle down to the periosteum. The periosteum was subsequently incised at 2 mm below the arcus marginalis, and access was gained to the fracture site in the orbital floor. Then, subperiosteal dissection was extended via the IOS to the orbital medial wall. This combined incision provided a wide opening for the surgical field and avoided detaching the inferior oblique muscle. After restoring the herniated soft tissues, the 3D-printed implant was inserted in the subperiosteal layer, and layer-by-layer closure was performed.

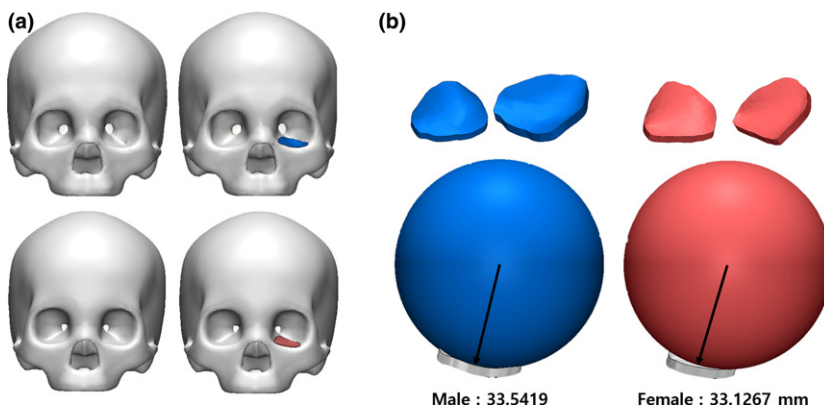


Fig. 1 (a) Korean male and female standard skull model. (b) Measurement of the radius of the sphere to contact the orbital wall using standard skull models of males and females. [Colour figure can be viewed at wileyonlinelibrary.com]

To analyze the outcome of the surgery, the symptoms were evaluated before and after surgery, and orbital volume was measured using CT at 3 days and 2 months after surgery.

Results

Quantifying the shape of the orbital inferomedial wall

The radius of the sphere in contact with the orbital wall was derived from the standard data, and measured 33.54 mm and 33.13 mm among males and females, respectively. The average radius of the sphere in contact with the orbital floor simulated the normal adult CT data, measuring 32.93 mm and 32.49 mm among adult males and females, respectively. As a result, the male-to-female ratio of the standard skull model was 98.76%, and that in a normal adult was 98.66% (Table 1). Although the radius was slightly different, it was confirmed that the dimensions of the sphere calculated for the males could fit the orbits of both males and females (Fig. 2). When the standardized model, designed by expanding to the medial wall, was simulated on the CT, it covered the orbits of both male and female patients well (Fig. 3). In addition, a difference of $\pm 200 \mu\text{m}$ was seen when the distance between the implant and the actual orbit was analyzed (Fig. 4).

Application of the standardized implant

Based on this result, a standardized 3D implant was created and applied to five patients with orbital complex fractures. The mean (range) follow-up period was 20.8 (18–27) months. The preoperative symptoms were diplopia accompanied by gaze discomfort and hypesthesia in one case, diplopia accompanied by hypesthesia in one case, and hypesthesia alone in two cases. The symptoms were all resolved (Table 2). The preoperative and postoperative CT were analyzed using Mimics (Materialize). Using repeated-measures one-way ANOVA, we compared the normal side volume (V_0) with the postoperative volume (V_{post}) and found them to be statistically similar. Using the same statistical approach, we identified statistically significant differences in V_0 compared to the preoperative volume (V_{pre}), and V_{pre} compared to V_{post} ($P < 0.05$; Fig. 5).

Table 1 Comparison of the radius of sphere measured in male and female standard models and in the actual orbital wall of patients

	Sphere radius from real patients, mm	Sphere radius from real standardized model, mm
Male	32.93 \pm 1.06	33.54
Female	32.49 \pm 1.02	33.13

Discussion

In the present study, orbital data obtained from 100 cadavers were used to create 3D printed implants, which were anatomically accurate and adequately covered by the simulation model. The radius of the sphere in contact with the orbit measured 33.54 mm, and was confirmed to be appropriate for the simulation model. The differences between the preoperative (V_{pre}), postoperative (V_{post}) and normal (V_0) orbital volumes were compared. V_0 and V_{post} were statistically similar, but the differences between V_0 and V_{pre} and between V_{pre} and V_{post} were statistically significant. On follow-up, the preoperative ocular symptoms were resolved.

Fractures of the IOS are seen frequently (Manolidis et al. 2002; Gooris et al. 2017) and can cause serious complications, including enophthalmos, orbital dystopia and double vision (Goldberg et al. 1992; Wright et al. 1999; Jordan & Anderson, 2000; Stathopoulos & Ameerally, 2018). The IOS is the important area in the orbit consisting of the thin bony junction of the orbital medial wall and floor (Yao et al., 2016), and an anatomical understanding of the IOS is essential for the reconstruction of the orbital bony structures (Burnstine, 2003; Jaquiere et al. 2007; Gart & Gosain, 2014; Bartoli et al. 2015).

The IOS is a conceptual structure consisting of adjacent orbital bones (Kim et al. 2002). It is referred to as the internal buttress of the orbits and strengthens the connection of the orbital medial wall and floor (Cornelius et al. 2014). It can be divided into three portions; the anterior IOS is formed by the maxillary bone with a small portion of the lacrimal bone, the midportion of the IOS is the junction of the maxillary bone and ethmoid bone, supported by the aerated ethmoid bone, and the posterior IOS is a triangular bone formed by the junction of the palatine and ethmoid bones, supported by the palatine bone. The total (range) length of the IOS, as measured from the orbital rim to the posterior margin of the palatine bone, was 37.6 (34–41) mm (Kim et al. 2002).

The orbital fracture is reconstructed with the aim of restoring the normal orbital volume by placing the fractured segment in an anatomically appropriate position. However, it is challenging to restore the delicate anatomy of the orbit precisely (Kim et al. 2002). It is essential to adapt the shape and position of the implant precisely to the premorbid bony contour (Stoor et al. 2014) because the accurate insertion of the implant allows restoration of optimal orbital volume and accurate form and position of the eye.

Inorganic implants, such as metal or polymer implants, have been used in the reconstruction of the orbital fracture (Ono et al. 1994; Cordewener et al. 1996; Dietz et al. 2001; Tuncer et al. 2007; Xu et al. 2009) Although the shape of the implant can be easily tailored, it is

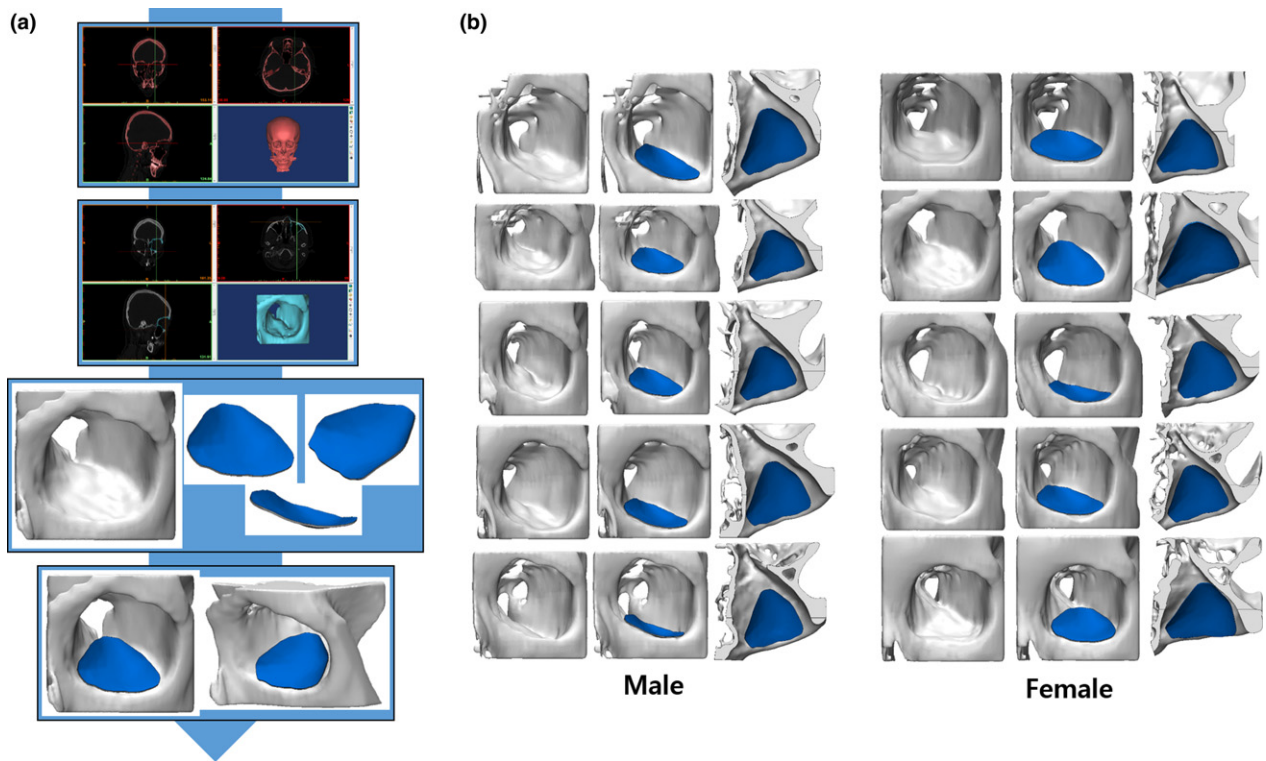


Fig. 2 (a) Process of visualizing the two-dimensional data from the computed tomography of the patient as a three-dimensional (3D) model. (b) Comparison between Korean standardized orbital mesh implant and 3D simulation model. [Colour figure can be viewed at wileyonlinelibrary.com]

difficult to bend it accurately to achieve the exact contour as that before the injury. Inaccurate insertion of the implant can lead to complications, such as diplopia,

enophthalmos, exophthalmos or restricted globe movement (Shin et al., 2013). In addition, insertion and withdrawal of the implant several times to determine the

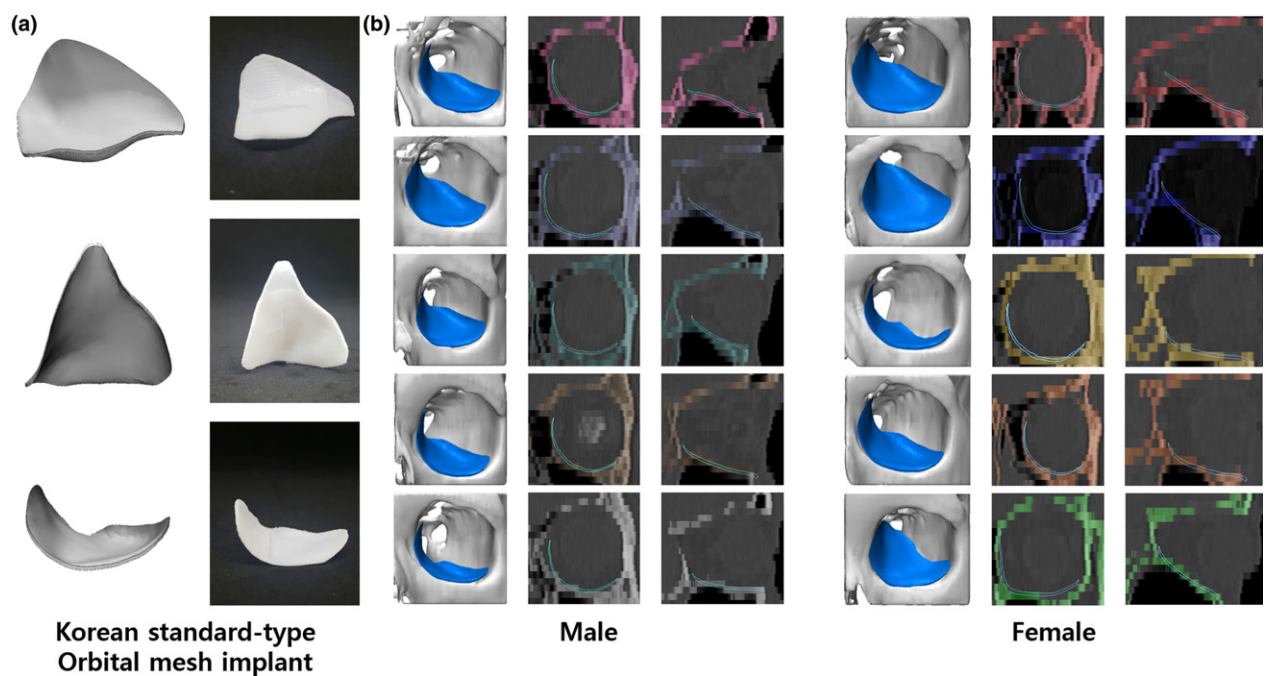


Fig. 3 (a) Korean standard-type orbital implant manufactured using a three-dimensional (3D) printer. (b) Comparison between the Korean standardized orbital implant and 3D model of actual patients. [Colour figure can be viewed at wileyonlinelibrary.com]

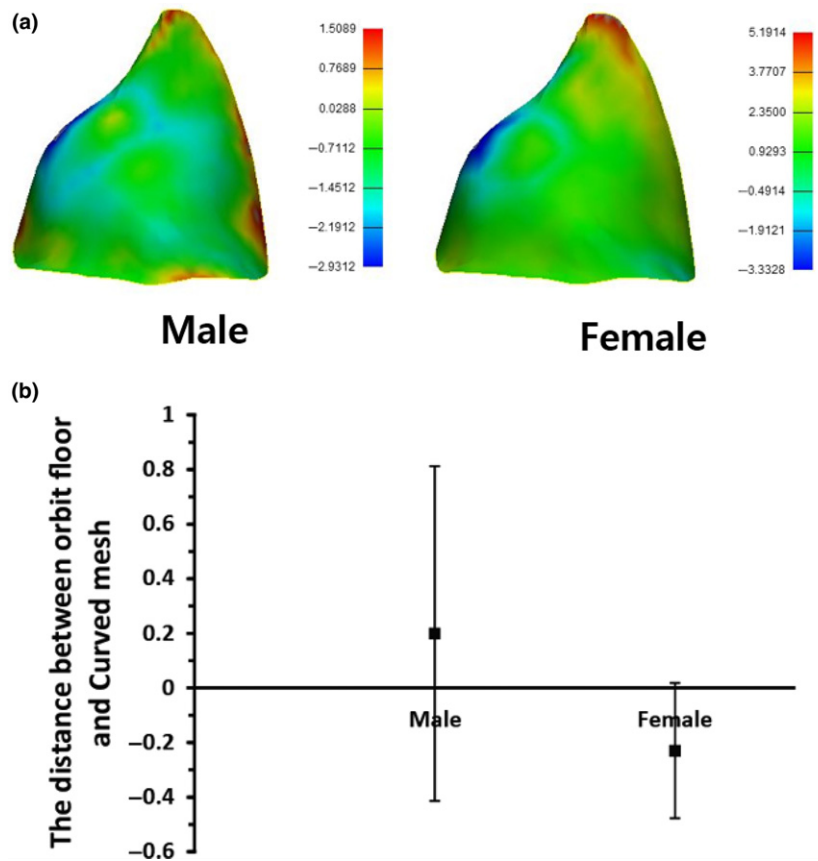


Fig. 4 Analysis of the differences between the orbital implant and orbital wall among Koreans using triangular points of implant. (a) Colored differences between the Korean orbital mesh implant and orbital wall of actual patients. (b) Differences between Korean orbital mesh implant and orbital wall of actual patients using numerical data. [Colour figure can be viewed at wileyonlinelibrary.com]

accuracy can result in an iatrogenic injury to the surrounding tissue (Kim et al. 2017).

Engineering techniques, including a rapid prototyping (RP) model, a mirrored patient-specific implant (PSI), and 3D printing technology, have been introduced in medicine to obtain a more precise implant contour (Hassfeld & Muhling, 2001; Metzger et al. 2006; Lieger et al. 2010; Stoor et al. 2014; Kozakiewicz, 2014; Gander et al. 2015; Oh et al. 2016; Cha et al. 2017; Kim et al. 2017; Vignesh et al. 2017) RP and a mirrored PSI are highly applicable to surgery because they easily produce a complex structure similar to an orbital

cavity. Aseptic treatment of the RP contour model is followed by intra-operative molding and bending of the implant material, such as titanium, to obtain a customized implant with a precise contour that is applied at the fracture site (Vehmeijer et al. 2016; Kronig et al. 2016; Oh et al. 2016; Kim et al. 2017). A mirrored PSI is obtained by 3D reconstruction of the fractured orbit using the mirrored normal orbit as a template (Gander et al. 2015).

Although RP and mirrored PSI can be used more accurately than implants that require manual bending, they require the creation of a contour model before surgery,

Table 2 Results among patients who applied standardized three-dimensional printing implant.

Patient number	V0, mm ³	V _{pre} , mm ³	V _{post} , mm ³	Preoperative symptoms	Postoperative symptoms	Follow-up period
1	24 812	28 543	25 980	(-)	(-)	3
2	28 342	32 318	30 880	Gaze discomfort, diplopia and hypesthesia	(-)	10
3	25 222	28 529	25 167	Hypesthesia	(-)	1
4	21 788	24 166	22 882	Hypesthesia	Hypesthesia	2
5	23 602	31 105	25 412	Diplopia, hypesthesia	Hypesthesia	2
Mean	24 753.20	28 932.20	26 064.20			3.6

Abbreviations: V0, normal side volume; V_{pre}, preoperative volume; V_{post}, postoperative volume.

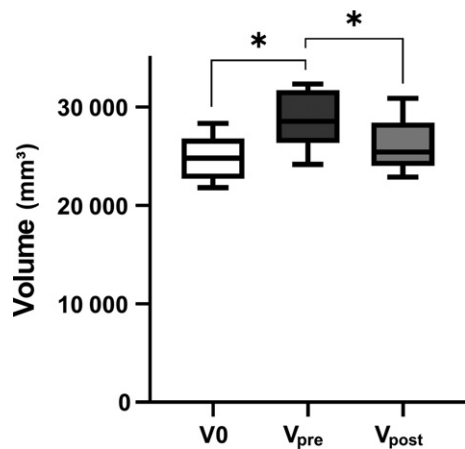


Fig. 5 Analysis of orbital volume in preoperative and postoperative computed tomography. According to the result of repeated measured one-way ANOVA, normal side volume (V_0) and postoperative volume (V_{post}) were similar, but differences between V_0 and preoperative volume (V_{pre}), as well as V_{pre} and V_{post} were significant ($P < 0.05$).

resulting in additional cost and preparation time. Furthermore, engineers need to be involved to produce an individualized model for each procedure. Because an orbital fracture is a common facial fracture, a ready-made standardized implant with a precise anatomical contour is advantageous for practical application without additional cost, time and labor. The focus of the present study, therefore, was on obtaining the anatomical dimensions of the orbit, especially of the complicated structure of the IOS, because a ready-made implant is needed to overcome the lack of structural support in the fractured IOS (Su & Harris, 2006; Hur et al. 2015).

It began with the extraction of the shape of the IOS from an average skull model. The Korean standard data were obtained from the Korean Human Model Database (<http://dk.kisti.re.kr>) at the KISTI (Seung-Ho et al. 2006). The orbit medial wall through the IOS and orbital floor were extracted from the Korean standard data of the skull using 3-matic (Materialize), and the implant was designed so that the contour would precisely fit onto the surface of the orbit. The standardization was confirmed through a simulation model, and this implant was found to have the same benefits as creating an implant with a pre-morbid CT scan. This design can be mass produced and standardized to meet the characteristics of Korean patients; it also reduces the manufacturing time, cost and manpower, and can be applied clinically.

The design of the implant conformed to the orbital medial wall and floor in the simulation using the CT scans of patients with orbital fractures. The 3D printing technology allows the implant to be manufactured precisely shaped, without any errors caused by manual bending. In addition, compared to the conventional pre-bent implants using RP, mass production is possible without additional labor, cost and time.

Eventually, the status of the standardized implant is between a manual-bending implant and PSI through RP. However, it attempted to contain the anatomical accuracy of the orbital cavity by reproduction of the orbital infero-medial wall, including the IOS, and the results were derived from simulation and actual patient surgery. Further, this is the first study to incorporate cadaveric anatomy data into 3D printing technology. Clinical data are still scarce, and the product of this study needs to be applied to more patients with complex orbital fractures. Data from clinical environments can weigh the pros and cons of using the standardized 3D-printed implant. This might be a satisfactory bridging strategy until technological advancements make in-house printing of the PSI possible.

Polycaprolactone is a non-toxic, degradable, biocompatible and absorbent polymer that does not produce harmful byproducts (Cho, 2014; Teo et al. 2015). It is approved by the US Food and Drug Administration for use in various devices for medical applications, including implants, drug delivery devices, and sutures (Place et al. 2009; Stewart et al. 2018). PCL implants will disintegrate after more than 2 years (Gunatillake & Adhikari, 2003), stimulating osteogenesis. Mesh implants made of PCL have ingrowth of fibrovascular tissue before they are absorbed, leading to reduced infection, exposure and dislocation (Dougherty & Wellisz, 1994). PCL is non-abrasive and rarely shows extrusion. It is radiolucent and shows low restitution with semi-rigid materials and structural stability. Many studies have shown no difference in the results between absorbable and non-absorbable implants in orbital wall reconstruction, and no significant differences are seen in long-term follow-up, which means that PCL is sufficient as an implant for orbital reconstruction (Hwang & Kim, 2010; Baek et al. 2014).

In conclusion, the orbital data, extracted from 100 CT scans of cadavers, provide standardized orbital anatomy and are the basis for construction of 3D printed implants. The design of the implants adequately covered the simulation model and showed satisfactory results when applied clinically in actual patients. It is anatomically accurate in the orbital cavity and can provide a sufficient bridging strategy until the in-housing printing technology of PSI is developed.

Acknowledgements

This work was financially supported by National Research Foundation of Korea, funded by the Ministry of Education (2017M3A9E2060428 and 2017R1C1B5017773), and by 'Supporting Project to evaluation New Domestic Medical Devices in Hospitals' funded by the Ministry of Health and Welfare and Korea Health Industry Development Institute.

Conflict of interest

None declared.

Data availability statement

N/A.

References

- Baek WI, Kim HK, Kim WS, et al. (2014) Comparison of absorbable mesh plate versus titanium-dynamic mesh plate in reconstruction of blow-out fracture: an analysis of long-term outcomes. *Arch Plast Surg* **41**, 355–61.
- Bartoli D, Fadda MT, Battisti A, et al. (2015) Retrospective analysis of 301 patients with orbital floor fracture. *J Craniomaxillofac Surg* **43**, 244–7.
- Burnstine MA (2003) Clinical recommendations for repair of orbital facial fractures. *Curr Opin Ophthalmol* **14**, 236–40.
- Cha JH, Moon MH, Lee YH, et al. (2017) Correlation between the 2-dimensional extent of orbital defects and the 3-dimensional volume of herniated orbital content in patients with isolated orbital wall fractures. *Arch Plast Surg* **44**, 26–33.
- Cordewener FW, Bos RR, Rozema FR, et al. (1996) Poly(L-lactide) implants for repair of human orbital floor defects: clinical and magnetic resonance imaging evaluation of long-term results. *J Oral Maxillofac Surg* **54**(1), 9–13.
- Cornelius CP, Mayer P, Ehrenfeld M, et al. (2014) The orbits—anatomical features in view of innovative surgical methods. *Facial Plast Surg* **30**, 487–508.
- Dietz A, Ziegler CM, Dacho A, et al. (2001) Effectiveness of a new perforated 0.15 mm poly-p-dioxanon-foil versus titanium-dynamic mesh in reconstruction of the orbital floor. *J Maxillofac Surg* **29**, 82–88.
- Dougherty WR, Wellisz T (1994) The natural history of alloplastic implants in orbital floor reconstruction: an animal model. *J Craniofac Surg* **5**, 26–32.
- Gander T, Essig H, Metzler P, et al. (2015) Patient specific implants (PSI) in reconstruction of orbital floor and wall fractures. *J Craniomaxillofac Surg* **43**, 126–30.
- Gart MS, Gosain AK (2014) Evidence-based medicine: orbital floor fractures. *Plast Reconstr Surg* **134**, 1345–55.
- Goldberg RA, Shorr N, Cohen MS (1992) The medical orbital strut in the prevention of postdecompression dystopia in dysthyroid ophthalmopathy. *Ophthalmic Plast Reconstr Surg* **8**, 32–4.
- Gooris PJJ, Muller BS, Dubois L, et al. (2017) Finding the ledge: sagittal analysis of bony landmarks of the orbit. *J Oral Maxillofac Surg* **75**, 2613–2627.
- Gunatillake PA, Adhikari R (2003) Biodegradable synthetic polymers for tissue engineering. *Eur Cell Mater* **5**, 1–16.
- Hassfeld S, Muhling J (2001) Computer assisted oral and maxillofacial surgery—a review and an assessment of technology. *Int J Oral Maxillofac Surg* **30**, 2–13.
- Hur SW, Kim SE, Chung KJ, et al. (2015) Combined orbital fractures: surgical strategy of sequential repair. *Arch Plast Surg* **42**, 424–30.
- Hwang K, Kim DH (2010) Comparison of the supporting strength of a poly-L-lactic acid sheet and porous polyethylene (Medpor) for the reconstruction of orbital floor fractures. *J Craniofac Surg* **21**, 847–53.
- Jaquiere C, Aeppli C, Cornelius P, et al. (2007) Reconstruction of orbital wall defects: critical review of 72 patients. *Int J Oral Maxillofac Surg* **36**, 193–9.
- Jordan DR, Anderson RL (2000) Orbital decompression. *Ophthalmic Plast Reconstr Surg* **16**, 167–8.
- Kim JW, Goldberg RA, Shorr N (2002) The inferomedial orbital strut: an anatomic and radiographic study. *Ophthalmic Plast Reconstr Surg* **18**, 355–64.
- Kim YC, Jeong WS, Park TK, et al. (2017) The accuracy of patient specific implant presented with 3D-printed rapid prototype model for orbital wall reconstruction. *J Craniomaxillofac Surg* **45**, 928–936.
- Kozakiewicz M (2014) Computer-aided orbital wall defects treatment by individual design ultrahigh molecular weight polyethylene implants. *J Craniomaxillofac Surg* **42**, 283–9.
- Kronig SA, van der Mooren RJ, Strabbing EM, et al. (2016) Pure orbital blowout fractures reconstructed with autogenous bone grafts: functional and aesthetic outcomes. *Int J Oral Maxillofac Surg* **45**, 507–12.
- Lee S-H, Lee JH, Cho Y-S (2014) Analysis of degradation rate for dimensionless surface area of well-interconnected PCL scaffold via in-vitro accelerated degradation experiment. *Tissue Eng Regen Med* **11**, 446–452.
- Lieger O, Richards R, Liu M, et al. (2010) Computer-assisted design and manufacture of implants in the late reconstruction of extensive orbital fractures. *Arch Facial Plast Surg* **12**, 186–91.
- Manolidis S, Weeks BH, Kirby M, et al. (2002) Classification and management of orbital fractures: experience with 111 orbital reconstructions. *J Craniofac Surg* **13**(6), 726–737.
- Metzger MC, Schon R, Weyer N, et al. (2006) Anatomical 3-dimensional pre-bent titanium implant for orbital floor fractures. *Ophthalmology* **113**, 1863–8.
- Oh TS, Jeong WS, Chang TJ, et al. (2016) Customized orbital wall reconstruction using three-dimensionally printed rapid prototype model in patients with orbital wall fracture. *J Craniofac Surg* **27**, 2020–2024.
- Ono I, Gunji H, Suda K, et al. (1994) Orbital reconstruction with hydroxyapatite ceramic implants. *Scand J Plast Reconstr Surg Hand Surg* **28**, 193–8.
- Place ES, George JH, Williams CK, et al. (2009) Synthetic polymer scaffolds for tissue engineering. *Chem Soc Rev* **38**, 1139–51.
- Seung-Ho HDSK, U-Young L, Kwang-Nam C, et al. (2006) Digital Korean human model database. *J Korean Soc Precis Eng* **21**, 37–40.
- Shin JW, Lim JS, Yoo G, et al. (2013) An analysis of pure blow-out fractures and associated ocular symptoms. *J Craniofac Surg* **24**, 703–7.
- Stathopoulos P, Ameerally P (2018) Reconstructing a traumatic empty orbit: principles, difficulties of treatment, and literature review. *J Oral Maxillofac Surg* **76**(9), 1952.e1–1952.e4.
- Stewart SA, Dominguez-Robles J, Donnelly RF, et al. (2018) Implantable polymeric drug delivery devices: classification, manufacture, materials, and clinical applications. *Polymers* **10**(12), 1379.
- Stoor P, Suomalainen A, Lindqvist C, et al. (2014) Rapid prototyped patient specific implants for reconstruction of orbital wall defects. *J Craniomaxillofac Surg* **42**, 1644–9.
- Su GW, Harris GJ (2006) Combined inferior and medial surgical approaches and overlapping thin implants for orbital floor and medial wall fractures. *Ophthalmic Plast Reconstr Surg* **22**, 420–3.
- Teo L, Teoh SH, Liu Y, et al. (2015) A novel bioresorbable implant for repair of orbital floor fractures. *Orbit* **34**, 192–200.

- Tuncer S, Yavuzer R, Kandal S, et al.** (2007) Reconstruction of traumatic orbital floor fractures with resorbable mesh plate. *J Craniofac Surg* **18**, 598–605.
- Vehmeijer M, van Eijnatten M, Liberton N, et al.** (2016) A Novel method of orbital floor reconstruction using virtual planning, 3-dimensional printing, and autologous bone. *J Oral Maxillofac Surg* **74**, 1608–12.
- Vignesh U, Mehrotra D, Dichen,, Anand V, Howlader D.** (2017) Three dimensional reconstruction of late post traumatic orbital wall defects by customized implants using CAD-CAM, 3D stereolithographic models: a case report. *J Oral Biol Craniofac Res* **7**, 212–218.
- Wright ED, Davidson J, Codere F, et al.** (1999) Endoscopic orbital decompression with preservation of an inferomedial bony strut: minimization of postoperative diplopia. *J Otolaryngol* **28**, 252–6.
- Xu JJ, Teng L, Jin XL, et al.** (2009) Porous polyethylene implants in orbital blow-out fractures and enophthalmos reconstruction. *J Craniofac Surg* **20**, 918–20.
- Yao WC, Sedaghat AR, Yadav P, et al.** (2016) Orbital decompression in the endoscopic age: the modified inferomedial orbital strut. *Otolaryngol Head Neck Surg* **154**, 963–9.